Drilling Task with a Quadruped Robot for Silage Face Measurements

Viviana Morlando
DIETI
University of Naples Federico II
Naples, Italy
viviana.morlando@unina.it

Gianluca Neglia
DMVPA
University of Naples Federico II
Naples, Italy
neglia@unina.it

Fabio Ruggiero
DIETI
University of Naples Federico II
Naples, Italy
fabio.ruggiero@unina.it

***Abstract*—Robotic systems are starting to be used not only within industrial environments but also in the agricultural field. To meet the increasing requirements of optimising monitoring and management, automation in the livestock field has noticeably increased in the last few years. However, robotics solutions still need to find their space in this field. In order to propose a possible application of robotic technologies for monitoring animals' health, this paper proposes the employment of a quadruped robot for drilling a silage face to analyse the silage quality. The study is performed through the dynamic simulator *Gazebo*.**

***Index Terms*—quadruped robot, silage, coring, whole-body control**

I. Introduction

Over the years, robotics has become more and more involved in assisting human beings by performing typically dull, dangerous, or repetitive tasks. Recently, service robotics has seen significant development, starting to spread robotic systems in challenging and complex environments apart from industrial ones. To meet the increasing requirements of optimising monitoring and management, automation in the livestock field has noticeably increased in the last few years. In agriculture and livestock, robotics application is challenging for several reasons. Usually, livestock is maintained in open environments, such as pasture or paddock, leading to practical difficulties. Furthermore, animals could be scared of these new technologies or, in other cases, be intrigued by them, causing either their break or malfunction. However, some specific robotic technologies are already used in livestock to reduce human labour and improve animal and environmental performances. For example, in dairy cattle, and in the last few years also in dairy buffaloes, the adoption of automated milking systems (AMS) has shown a noticeable increase in their positive effects on animal welfare and production efficiency (for review [1]). In this sense, AMS entrepreneurial groups estimated that by 2025 about 50% of dairy cattle farms would use an AMS [2]. Robotic technologies have also been used to improve manure management systems through scrapers [3] or for managing the animals at pasture through robotic quadrupeds [4]. However, the last technology is only applied from an experimental point of view. Robotic technologies are also starting to be employed to monitor animals' health and quality of life.

The research leading to these results has been supported by the COWBOT project, in the frame of the PRIN 2020 research program, grant number 2020NH7EAZ_002, and the Agritech National Research Center and received funding from the European Union Next-GenerationEU (PIANO NAZIONALE DI RIPRESA E RESILIENZA (PNRR) – MISSIONE 4 COMPONENTE 2, INVESTIMENTO 1.4 – D.D. 1032 17/06/2022, CN00000022). This manuscript reflects only the authors' views and opinions, neither the European Union nor the European Commission can be considered responsible for them.

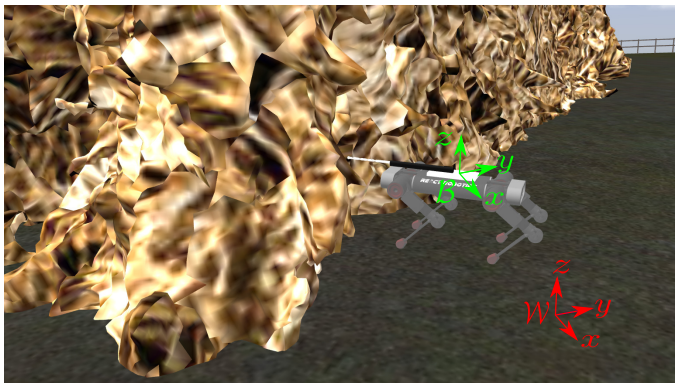

Fig. 1. Representation in the simulation environment of a quadruped robot involved in a drilling task with a silage face. Relevant world (in red) and body (in green) frames are also represented.

For this reason, this paper proposes employing a quadruped robot for drilling tasks in an agricultural environment. The robot is supposed to accomplish the coring of a silage face to analyse the silage quality. Automating the silage coring is meaningful to accomplish the possibility of continuous and fast monitoring of the animals' food within a farm. This study is realised through simulations, and the main objective is to be able to impress a force of at least 70 N on a silage wall.

II. Devised Framework

The quadruped robot must interact with the silage face safely to perform the drilling task. The main challenge during this operation is to retain the robot's balance despite the high reaction force acting on the structure because of the interaction. In order to perform the drilling with no slipping of the robot's feet on the ground, the solution employed in this paper is a whole-body controller. Such a kind of controller allows computing the commands to send to the robot to move it with the desired behaviour, exploiting the full capabilities of

the entire body. The desired behaviour of the robot is chosen not only to impress the desired force on the silage face but also to have no sliding of the feet on the ground. The controller includes an optimization problem to find the best solution to obtain this behaviour. Since the primary concern during the drilling task comes from the reaction forces of the interaction on the robot's trunk that could unbalance the robot itself, a disturbance observer is also employed within the controller. The disturbance observer estimates external forces acting on the robot, allowing it to compensate for and reject them during the computation of the robot's commands.

A. Mathematical model formulation

Legged robots are usually modelled as a free-floating base with some legs attached. Let B be the frame whose position is attached to the robot's CoM and whose orientation is the one of a fixed frame on the main body, and let W be the fixed world frame (Fig. 1), respectively. The free-floating base is modelled through 6 virtual joints giving 6 degrees of freedom (DoFs) with respect to W. Moreover, n_l 2 legs are attached to the floating base, giving other nn_l DoFs to the structure, with $n > 0$ joints for each leg. Let $x_{com} = \begin{bmatrix} x_c & y_c & z_c \end{bmatrix}^\mathsf{T}$ 2 R^3, $\dot{x}_{com}$ 2 R^3, and $\ddot{x}_{com}$ 2 R^3 be the position, velocity, and acceleration of the frame B's origin with respect to W, respectively. Besides, let $!_{com}$ 2 R^3 and $!_{com}$ 2 R^3 be the angular velocity and the angular acceleration of B with respect to W, respectively. The orientation of B with respect to W is expressed by the rotation matrix R_b 2 $SO(3)$, from which it can be extracted the set of ZYX Euler angles 2 R^3. Finally, indicate with q 2 R^{nn_l} the vector collecting the legs' joints. The dynamic model of a legged robot can be formulated in terms of the global CoM through the transformation introduced in [5]. A decoupled structure for the dynamic model is obtained [6]–[8] through this transformation, and assuming that the main's body angular motion is slow. Considering that $M_{com;a}$ is the inertia matrix related to the main's body angular motion, through this last assumption, $\frac{d}{dt}(M_{com;a}!_{com}) = M_{com;a}!_{com}$ holds, meaning that the effect of precession and nutation of the rotating body are discarded [8]. The inertia matrix is $M(q) = \begin{bmatrix} M_{com;l}(q) & O_{3\ 3} & O_{3\ nn_l} \\ O_{3\ 3} & M_{com;a}(q) & O_{3\ nn_l} \\ O_{nn_l\ 3} & O_{nn_l\ 3} & M_q(q) \end{bmatrix}$ 2 $\mathsf{R}^{(6+nn_l)\ (6+nn_l)}$; the vector accounting for Coriolis, centripetal, and gravitational forces is $h(q; \ ) = \begin{bmatrix} O_{6\ (6+nn_l)} \\ C_q(q; \ ) \end{bmatrix} + \begin{bmatrix} mg \\ 0_{nn_l} \end{bmatrix}$, with $C_q(q; \ )$ 2 $\mathsf{R}^{nn_l\ (6+nn_l)}$, where $= \begin{bmatrix} \dot{x}_{com}^\mathsf{T} & !_{com}^\mathsf{T} & \dot{q}^\mathsf{T} \end{bmatrix}^\mathsf{T}$ 2 R^{6+nn_l} is the stacked velocity; $m > 0$ is the total mass of the robot, $g = \begin{bmatrix} g_0^\mathsf{T} & 0_3^\mathsf{T} \end{bmatrix}^\mathsf{T}$ 2 R^6, and g_0 2 R^3 the gravity vector; 0 and O the zero vector and matrix of proper dimensions. The resultant model is

$$M(q)\dot{} + h(q; \ ) = S^\mathsf{T} \ + J_{st}(q)^\mathsf{T} f_{gr} + J(q)^\mathsf{T} f_e + \\ + S_w^\mathsf{T} w_{e;c}; \quad (1)$$

with $S = \begin{bmatrix} O_{nn_l\ 6} & I_{nn_l} \end{bmatrix}$ the selection matrix of the actuated part; 2 R^{nn_l} the joint actuation torques; f_{gr} 2 $\mathsf{R}^{3n_{st}}$ the ground reaction forces that can be obtained by embedded sensors on robot's feet, with $0 < n_{st} \ n_l$ the number of stance legs; f_e 2 R^{3n_l} the stacked vector containing the resultant external force at the legs' tips; $S_w = \begin{bmatrix} I_{6\ 6} & O_{6\ nn_l} \end{bmatrix}$ the selection matrix of the unactuated part; $w_{e;c} = \begin{bmatrix} f_{e;c}^\mathsf{T} & \ _{e;c}^\mathsf{T} \end{bmatrix}^\mathsf{T}$ 2 R^6 the external wrench acting directly on the CoM (it is assumed that the external torques resulting at the legs' tip are negligible); $J_{st}(q) = \begin{bmatrix} J_{st;com}(q) & J_{st;j}(q) \end{bmatrix}$ 2 $\mathsf{R}^{3n_{st}\ 6+nn_l}$ and $J(q) = \begin{bmatrix} J_{com}(q) & J_j(q) \end{bmatrix}$ 2 $\mathsf{R}^{3n_l\ 6+nn_l}$ Jacobian matrices that are defined in [6]. It can be noticed that the CoM's dynamics are included in the first six rows of (1), decoupled from the legs' dynamics included in the other nn_l rows. It should be noticed that the resultant external forces at the legs' tip, f_e, can be considered as contacts that dictates a net wrench on the CoM, while the wrench directly applied to the CoM, $w_{e;c}$, influences only the CoM's dynamics.

B. Hyrid observer for external forces

Employing the decoupled structure of the legged robot's dynamics (1), the hybrid observer presented in [9] is used to estimate and reject the forces acting on the CoM and those on the legs. The disturbance rejection is one of the main aspects of the successful performance of the fronted task. The robot must overcome different challenges to retain its balance during the operation in an agricultural environment. One of these challenges is to handle the forces acting on the robot during the interaction with the silage face. The silage reacts to the driller thrust, creating an external force acting on the robot. In order to retain the balance against this force, a first observer on the CoM is used. The design of the estimator for the torque acting on the CoM in the time domain is [9]

$$\hat{}_c(t) = K_a \left(\ (t) \quad \int_0^t (\hat{}_c(\ ) + J_{st;com;a}^\mathsf{T} f_{gr}) \mathrm{d} \ \right); \quad (2)$$

where $\hat{}_c$ is the estimated external torque acting on the CoM, and is the generalized angular momentum. The design of the estimator for the linear force acting on the CoM in the time domain is instead [9]

$$\hat{f}_c(t) = K_l \int_0^t (M_{com,l}\ddot{x}_{com} + mg - J_{st,com,l}^\mathsf{T} f_{gr} - \hat{f}_c) \mathrm{d}\sigma, \quad (3)$$

where $\hat{f}_c$ is the estimation of the force.

A second challenge for the robot's balance is related to the external forces acting on the legs, given by the irregularities of the ground or the collision with an external object, such as the silage face itself. For this reason, a momentum-based observer acting on the robot's legs, presented in [6], is employed. The estimator can be written as

$$\hat{f}_j(t) = K_{2;j} \int_0^t (\ \hat{f}_j(\ ) + K_{1;j}(\ _j(t) \quad \int_0^t (\hat{f}_j(\ ) + C_q^\mathsf{T}\dot{q} + \\ + \ + J_{st;j}^T f_{gr}) \mathrm{d} \ )) \mathrm{d} \ ; \quad (4)$$

where $\hat{f}_j$ is the vector containing the external forces acting at the tip of each leg.

C. Motion planning

The motion is continuously replanned so that the ZMP is always maintained inside the support polygon [10]. From now on, the position and the orientation of the frame B will be stacked into $r_c = \left[x_{com}^{\mathsf{T}} \quad ^{\mathsf{T}}\right]^{\mathsf{T}} \; 2 \; \mathsf{R}^6$, while its velocity and acceleration can be considered $_c = \left[\dot{x}_{com}^{\mathsf{T}} \quad !_{com}^{\mathsf{T}}\right]^{\mathsf{T}} \; 2 \; \mathsf{R}^6$ and $\dot{}_c = \left[\ddot{x}_{com}^{\mathsf{T}} \quad !_{com}^{\mathsf{T}}\right]^{\mathsf{T}} \; 2 \; \mathsf{R}^6$. For each footstep, the motion is split into two phases, replanning the desired trajectory for the CoM at the beginning of each footstep, with a period $T_{fs} > 0$.

The motion planner computes the reference $r_{c;ref}$, $\dot{}_{c;ref}$ and $\ddot{}_{c;ref} \; 2 \; \mathsf{R}^6$ for the CoM and the reference $x_{sw;des} \; 2 \; \mathsf{R}^{3(n_l \; n_{st})}$ for the swing feet as a 3 rd order splines. Further details in [6].

D. Optimization problem

The wrench-based optimization problem used in this paper is based on [9]. Let $= \left[\dot{}_c^{\mathsf{T}} \quad \ddot{q}^{\mathsf{T}} \quad f_{gr}^{\mathsf{T}}\right]^{\mathsf{T}} \; 2 \; \mathsf{R}^{6+nn_l+3n_{st}}$ be the chosen control variables. The addressed problem has the following structure

$$\text{minimize} \quad f( ) \tag{5}$$

$$\text{subject to} \quad A \; = b; \tag{6}$$

$$D \quad c: \tag{7}$$

The details of each term of the above optimization problem can be found in [9]. The main difference of the controller used in this work regards the cost function $f( )$. The cost function tracks the CoM's reference pose, $r_{c;ref} \; 2 \; \mathsf{R}^6$, and the reference velocity and acceleration $_{ref}$ and $\dot{}_{c;ref}$, reducing as much as possible the control effort. To this aim, the desired wrench at the robot's CoM is computed using the first six equations of (1), as

$$w_{com;des} = K_p(r_{c;ref} \quad r_c) + K_d(\;_{c;ref} \quad \;_c) + mg + \\ + M_{com}(q)\,\dot{}_{c;ref}; \tag{8}$$

with $K_p; K_d \; 2 \; \mathsf{R}^{6 \; 6}$ positive definite matrices. Let $\hat{w}_{com} = \left[\hat{f}_c^{\mathsf{T}} \quad \hat{}_c^{\mathsf{T}}\right]^{\mathsf{T}}$ be the estimated external wrench at the CoM, the cost function minimizing the desired wrench and compensating for the disturbance can be written as $f( ) = \left\| J_{st;com}^{\mathsf{T}} \Sigma \quad (w_{com;des} \quad \hat{w}_{com}) \right\|_Q + \left\| \; \right\|_R$; with Q and R two symmetric and positive definite matrices that can be used to specify the relative weight between the components of the cost function, and $k \; k$ the quadratic form with proper matrix. The cost function refers to the impedance control strategy, modelling the contact dynamics as a virtual spring-damper system which can be described by a mass matrix, a damping matrix (K_d gain) and a stiffness matrix (K_p gain).

The main objective of the impedance control is to model the contact force between the end-effector and the environment, imposing an impedance behaviour through the damping and the stiffness gains.

In some cases, a robot could be involved in a different task, or the stiffness of the environment could change. This leads to the need to vary the impedance during the task, as is the case of the problem faced in this paper since the silage face has a variable density and pressure. Consequently, the stiffness could change during the execution of the task. The approach implemented to solve this problem is the variable impedance control [11]. The variable impedance control allows to modify the interaction behaviour based on the stiffness of the environment. In this case, it allows impressing enough force to perform the drilling task even when the density of the silage face becomes major. In order to realize a variable impedance control, the stiffness and the damping used in (8) are not fixed anymore, but they become time-depending $K_p(t)$ and $K_d(t)$. These gains are changed based on the feedback of the estimated external wrench. This wrench also gives information on the force impressed on the silage face. If this force is insufficient, the gains are changed to increase it.

III. Case studies

A. Simulation environment

The simulation features *DogBot*, an open-source platform from React Robotics. Each of the quadruped legs is equipped with three actuated revolute joints that enable lateral movement and hip and knee movements, allowing the lifting of the feet from the ground. With a weight of 21 kg, most of the robot's mass is concentrated in the body, weighing 12 kg, while each leg weighs 2 kg. Each leg's upper and lower segments have a length of approximately 0.3 m. The robot has been equipped with a driller to address the task at hand. The driller could have been installed using a manipulator arm with a driller end-effector. However, it was instead placed on the front of the main body (as shown in Fig. 1), allowing the robot to use its body weight to apply a significant force on the silage face through the combination of the drilling thrust and body push.

Gazebo was selected as the dynamic simulator due to its high-performance physics engine, which ensures a realistic representation of movement and external conditions. To further improve the realism of the simulation, an agricultural environment was chosen complete with uneven terrain. The environment also includes a silage face for the task to be performed on.

B. Silage face simulation

In order to simulate the contact between the driller and the silage in the best feasible way, some information about the silage wall must be introduced. The quality of the silage is mainly determined by its density [12]. Indeed, low-density values lead to high porosity and increase the losses during the use of the silage [13]. The density is primarily determined by how efficiently the material compaction is carried out. As a result of the ensilage process, the density of the silage increases along its thickness, meaning that, during the task, the driller will cope with a higher pressure while it goes deeper inside the wall. In order to replicate such behaviour during the simulation, the contact between the driller and the silage has been realized with a linearly variable friction coefficient that becomes higher where the density is significant. This

coefficient starts at $= 0.4$ on the silage surface, representing the interaction between aluminium and dry concrete, and increases linearly with the driller's penetration, reaching a maximum coefficient of $= 1$.

C. Description of the preliminary results

In this preliminary study, some simulations have been performed to verify the robot's capability to impress a desired force $F_d = 70$ N on the wall. Different parameters will be considered to understand the feasibility of the task:

The orientation of the robot. The simulations have been performed by changing the robot's angle. Then, the angle between the wall and the driller tool during the contact becomes the main parameter. The following will refer to it as an "inclination angle".

The friction coefficient of the ground. Three different values of the friction coefficient have been tested: $= 0.4$, $= 0.6$ and $= 0.8$. The variation in the friction coefficient results in varying degrees of slipperiness for the terrain. By simulating the task using different types of terrains with varying friction coefficients,the effectiveness of the framework can be evaluated.

D. Results: variation of the inclination angle

This section focuses on the results obtained from three different inclination angles, while considering a realistic friction coefficient of $= 0.6$, which simulates the contact between the robot's rubber feet and the field soil. The results are analysed in detail to assess the ability of the robot to generate the desired force under these conditions. Given the practicality of this friction coefficient, a thorough analysis of the results provides valuable insights into the performance of the robot. The results obtained are presented in Fig. 2. In Fig. 2a, the inclination angle is $= 0°$, meaning that the direction of the driller tool is normal to the silage surface. In Fig. 2b and Fig. 2c, instead, the angles are $= 28°$ and $= 57°$, respectively. It can be noticed that the impressed force F_w tends to maintain a constant trend and to be always over the desired 70 N in the first case. Differently in the other two cases, the force is higher with respect to the first one at the beginning. However, it has a decreasing trend in a second moment, unable to guarantee the desired force for a certain period. It can be deduced that having an inclination angle different from 0 makes the robot lose adequate gripping during the movement. In this case, the robot cannot have a constant force.

Then, analysing these preliminary results, the idea is that having a particular inclination guarantees an initial high force, given by the first impact between the robot and the wall. However, it does not allow to keep this force constant during the task because the robot is not pushing with its total weight. It can be noticed that the magnitude of the force alternates phases with a high force and phases with a relatively small force. The change of friction within the silage wall probably gives this behaviour. Differently, whenever the robot has a flat and constant orientation, normal to the wall, it can maintain

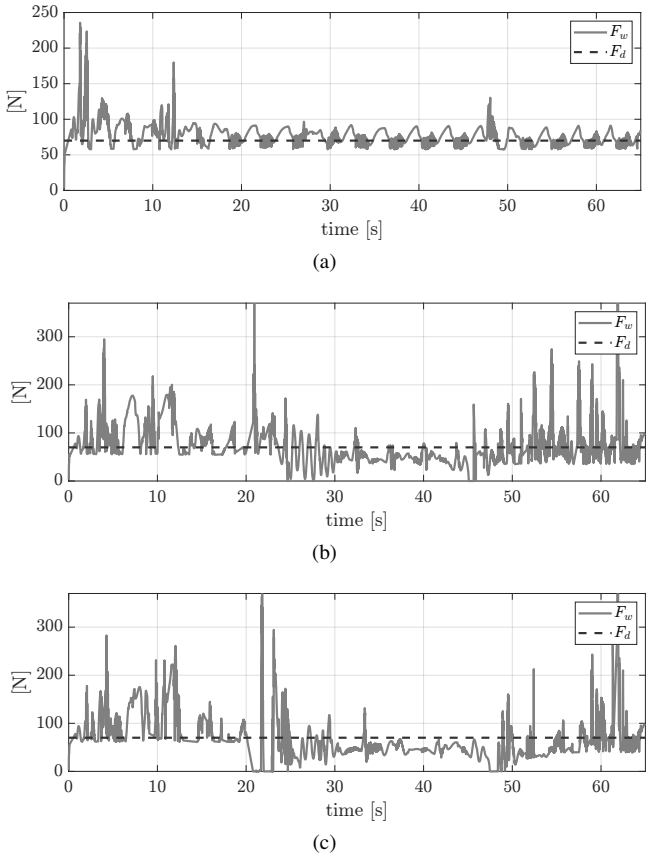

Fig. 2. Contact force obtained with different roll angles. (a) Roll angle $= 0°$ (b) Roll angle $= 28°$ (c) Roll angle $= 57°$

an adequate and almost constant force, probably because it pushes with the whole body.

E. Results: variation of the friction coefficient

This section analyzes the results obtained by varying the friction coefficient of the ground, using three different values: $= 0.4$, $= 0.6$, and $= 0.8$. Since the results demonstrated that the robot is capable of generating the desired force for all three friction coefficients, similarly to what is shown in Fig. 2, this section focuses on evaluating the robot's ability to maintain balance during the task.

Indeed, depending on the friction coefficient, the ground could become more or less slippery. For this reason, a robustness parameter can be employed [14], [15]

$$R(t) = 1 - H(t); \tag{9}$$

where, suppressing time dependencies to compact the notation, the function

$$H(\ ) = \sum_{i=1}^{n_c} H_i(\ _i) = \ ^1\sum_{i=1}^{n_c} \frac{1}{(\ _i \quad _i)(\ _i + \ _i)}; \tag{10}$$

is a measure related to how far the friction forces are from the friction cone boundaries, where $_i = \arctan$ is the semiaperture angle of the i th friction cone and $_i =$

$\arccos \hat{z}_i^{\mathsf{T}} f_{gr_{st;i}} / \|f_{gr_{st;i}}\|$ is the angle between the i-th contact normal $\hat{z}_i$ and the i-th stance leg, it was chosen $= 4$.

Let's begin by analysing the results obtained using a friction coefficient of $= 0.6$, which represents the most realistic scenario. In Fig. 3, we can observe the trend of the robustness parameter obtained for different inclination angles.

In this case, it can be observed that the robustness parameter remains consistently high throughout the entire task when the inclination angle is $= 0°$, as shown in Fig. 3. However, for different inclination angles, the robot's robustness decreases gradually, although the overall values of R are similar to those of the $= 0°$ case.

This indicates that when the inclination angle is different from zero, the robot's robustness decreases due to the fact that it becomes unbalanced as it reaches the desired roll angle.

To validate the performance of the robot, it's important to mention that we have also computed the average value of the robustness index in a stable configuration where the robot is not pushing against the wall and is in a stance position. The average robustness $\bar{R}$ can be computed as

$$\bar{R} = T^{-1} \int_0^T 1 / H(t)\, dt. \tag{11}$$

In the stable case, the average robustness was found to be $\bar{R} = 0.29$. From Fig. 3, it can be observed that the value of R remains relatively close to the one obtained in the stable case. The minor decrease in the index can be attributed to the robot needing to push against the wall to counteract the generated force. Despite this, the framework still maintains a high level of robustness even when the robot is pushing against the wall.

In Fig. 4, the average robustness $\bar{R}$ can be observed for the different friction coefficients within an interaction plot. Some general observation can be made:

Increasing the friction coefficient generally leads to an increase in robustness. This can be attributed to the fact that a higher friction coefficient results in less slippage of the ground, which helps the robot maintain its balance.
Varying , the robustness for $= 27°$ and $= 57°$ has a similar trend.
When considering high values of , such as $= 0.8$, there is a significant improvement in the average robustness $\bar{R}$ at $= 0°$ compared to the other two angles. This can be attributed to the fact that in this case, the robot maintains a flat attitude that, together with the higher friction coefficient, helps it to retain a robust balance without becoming unbalanced like in the other two cases.
When considering low values of , it is evident that the average robustness $\bar{R}$ deteriorates faster when the robot maintains a flat attitude compared to when it is at $= 27°$ or $= 57°$. This can be attributed to the fact that only in this case, the robot is able to exert a constant and higher force, which causes a major external disturbance. This external disturbance, combined with the slippery terrain, makes it more challenging for the robot to maintain a robust balance.

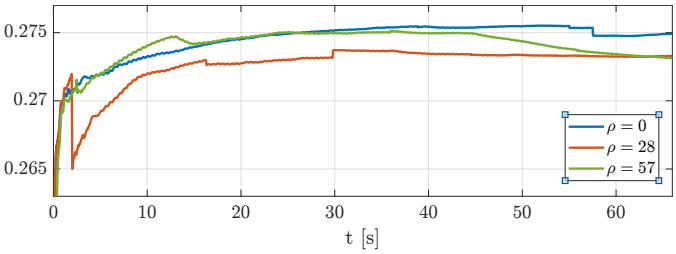

Fig. 3. Robustness index $\mathcal{R}$ obtained with $= 0.6$ and roll angles $= 0°$, $= 28°$ and $= 57°$

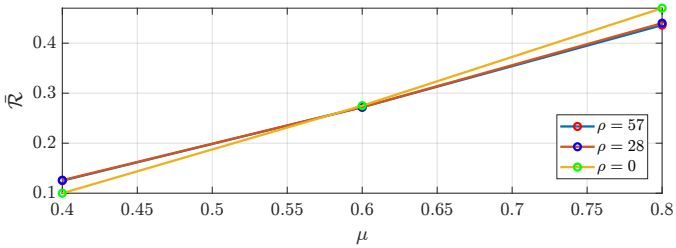

Fig. 4. Interaction plot of the Average Robustness index $\mathcal{R}$ obtained with $= 0.4$, $= 0.6$ and $= 0.8$ and roll angles $= 0°$, $= 28°$ and $= 57°$

The simulations performed in this study provide a preliminary investigation of the use of a whole-body controller with a quadruped robot for a drilling task. These results offer a general insight into the optimal configuration of the robot in various scenarios. Although the friction parameters are usually known in typical operating environments, they may vary due to meteorological changes. For instance, the ground could become wetter or drier, resulting in different friction coefficients. By using a method to estimate these coefficients [16], the robot can be configured to deliver optimal performance.

With further research, it may be possible to develop a policy to adapt not only the gains of the impedance control but also the position and orientation of the robot. This would enable the robot to maintain robustness even in uncertain environments, leading to enhanced operational reliability and versatility.

IV. Conclusion and Future Work

This study introduces a novel control architecture for a quadruped robot to perform a drilling task. The architecture includes a whole-body controller and an adaptive impedance control that models the interaction between the driller and the silage wall. The force that the robot can apply to the wall was evaluated, and the results showed that the required force could be achieved in most cases, although only the pushing force was considered, not the rotational thrust of the driller. To assess the robustness of the robot balance, the robot was tested on different types of soil with varying inclination angles. The results indicate that the best performance is generally achieved with a higher friction coefficient and a flat orientation. However, when the friction decreases, the robot

performs better with a different orientation. This suggests that the robot's orientation can be adapted depending on the scenario to achieve a balance between robustness and drilling force. Overall, these findings have important implications for adapting the robot's configuration in various situations and achieving optimal performance.

Based on the obtained results, there is potential for further analysis to enhance the robustness of the control strategy and make it adaptable to various precision livestock farming tasks. Specifically, future studies could consider the combined effect of the pushing force exerted by the robot and the rotational thrust of the driller. Such an analysis could provide insights on how to improve drilling efficiency without compromising the balance and stability of the robot.

Moreover, the adaptive impedance control used in this study could be further optimized to better model the dynamic interaction between the robot and the environment. This could lead to a more robust and efficient control strategy that can adapt to various environmental conditions.

Overall, these advancements could lead to a more flexible and adaptable robot control strategy that can be used for a variety of precision livestock farming tasks beyond drilling, such as crop monitoring, livestock management, and soil analysis.

REFERENCES

[1] A. Cogato, M. Brščić, H. Guo, F. Marinello, and A. Pezzuolo, "Challenges and tendencies of automatic milking systems (ams): A 20-years systematic review of literature and patents," *Animals*, vol. 11, no. 2, p. 356, 2021.

[2] B. G. Hansen, H. O. Herje, and J. Höva, "Profitability on dairy farms with automatic milking systems compared to farms with conventional milking systems," *International Food and Agribusiness Management Review*, vol. 22, no. 2, pp. 215–228, 2019.

[3] A. Chiumenti, F. da Borso, A. Pezzuolo, L. Sartori, and R. Chiumenti, "Ammonia and greenhouse gas emissions from slatted dairy barn floors cleaned by robotic scrapers," *Research in Agricultural Engineering*, vol. 64, no. 1, pp. 26–33, 2018.

[4] A. Torres-Pardo, D. Pinto-Fernández, M. Garabini, F. Angelini, D. Rodriguez-Cianca, S. Massardi, J. Tornero-López, J. C. Moreno, and D. Torricelli, "Legged locomotion over irregular terrains: State of the art of human and robot performance," *Bioinspiration & Biomimetics*, 2022.

[5] C. Ott, M. A. Roa, and G. Hirzinger, "Posture and balance control for biped robots based on contact force optimization," in *2011 11th IEEE-RAS International Conference on Humanoid Robots*, 2011, pp. 26–33.

[6] V. Morlando, A. Teimoorzadeh, and F. Ruggiero, "Whole-body control with disturbance rejection through a momentum-based observer for quadruped robots," *Mechanism and Machine Theory*, vol. 164, p. 104412, 2021.

[7] B. Henze, C. Ott, and M. Roa, "Posture and balance control for humanoid robots in multi-contact scenarios based on model predictive control," in *2014 IEEE/RSJ International Conference on Intelligent Robots and Systems*, 2014, pp. 3253–3258.

[8] J. Di Carlo, P. M. Wensing, B. Katz, G. Bledt, and S. Kim, "Dynamic locomotion in the mit cheetah 3 through convex model-predictive control," in *2018 IEEE/RSJ International Conference on Intelligent Robots and Systems*, 2018, pp. 1–9.

[9] V. Morlando and F. Ruggiero, "Disturbance rejection for legged robots through a hybrid observer," in *2022 30th Mediterranean Conference on Control and Automation (MED)*. IEEE, 2022, pp. 743–748.

[10] C. D. Bellicoso, F. Jenelten, P. Fankhauser, C. Gehring, J. Hwangbo, and M. Hutter, "Dynamic locomotion and whole-body control for quadrupedal robots," in *2017 IEEE/RSJ International Conference on Intelligent Robots and Systems*, 2017, pp. 3359–3365.

[11] F. J. Abu-Dakka and M. Saveriano, "Variable impedance control and learning—a review," *Frontiers in Robotics and AI*, vol. 7, p. 590681, 2020.

[12] A. M. Krüger, P. d. M. T. Lima, A. L. Abdalla Filho, J. de Geus Moro, I. Q. De Carvalho, A. L. Abdalla, and C. C. Jobim, "Dry matter concentration and corn silage density: Effects on forage quality," *Tropical Grasslands-Forrajes Tropicales*, vol. 8, no. 1, pp. 20–27, 2020.

[13] G. Borreani, E. Tabacco, R. Schmidt, B. Holmes, and R. Muck, "Silage review: Factors affecting dry matter and quality losses in silages," *Journal of Dairy Science*, vol. 101, no. 5, pp. 3952–3979, 2018.

[14] V. Morlando, M. Selvaggio, and F. Ruggiero, "Nonprehensile object transportation with a legged manipulator," in *2022 International Conference on Robotics and Automation (ICRA)*. IEEE, 2022, pp. 6628–6634.

[15] M. Selvaggio, J. Cacace, C. Pacchierotti, F. Ruggiero, and P. R. Giordano, "A shared-control teleoperation architecture for nonprehensile object transportation," *IEEE Transactions on Robotics*, vol. 38, no. 1, pp. 569–583, 2021.

[16] M. Focchi, V. Barasuol, M. Frigerio, D. G. Caldwell, and C. Semini, "Slip detection and recovery for quadruped robots," *Robotics Research: Volume 2*, pp. 185–199, 2018.